Orbital and spin magnetic quadrupole response in heavy nuclei

J. Kvasil,[1] N. Lo Iudice,[2] V. O. Nesterenko,[3] A. Macková,[1,4] and P. Alexa[5]
[1]*Department of Nuclear Physics, Charles University, CS-18000 Prague 8, Czech Republic*
[2]*Dipartimento di Scienze Fisiche, Università di Napoli ''Federico II,'' Monte S. Angelo, Via Cinzia I-80126 Napoli, Italy and Istituto Nazionale di Fisica Nucleare Monte S. Angelo, Via Cinzia I-80126 Napoli, Italy*
[3]*Bogoliubov Laboratory of Theoretical Physics, Joint Institute for Nuclear Research, 141980 Dubna, Moscow region, Russia*
[4]*Institute of Nuclear Physics, Czech Academy of Science, Rez near Prague, Czech Republic*
[5]*Institute of Physics and Measuring Technique, Chemical Technical University Technická 3, CS-16000 Prague 6, Czech Republic*
(Received 28 July 2000; revised manuscript received 8 January 2001; published 10 April 2001)

We compute the magnetic quadrupole strength function in heavy spherical and deformed nuclei in proton-neutron random-phase approximation using a separable Hamiltonian that couples magnetic and electric channels and adopting a technique that avoids the diagonalization of the eigenvalue matrix. We intend to check if the different sensitivity of the spin dipole and orbital responses to the multipole terms of the Hamiltonian leads to an energy separation of the two modes sufficient for the identification of the *twist* mode. We explore also the possibility of a K splitting induced by deformation, in analogy to the electric giant dipole resonance, also briefly studied for the sake of completeness.

DOI: 10.1103/PhysRevC.63.054305 PACS number(s): 21.60.Jz, 23.20.Js, 25.20.Dc

I. INTRODUCTION

The massive studies of magnetic dipole ($M1$) transitions have contributed to clarify the origin of quenching and fragmentation of the spin strength in nuclei [1], a longstanding problem that seems to have made important advances in recent years [2–4]. Moreover, they have led to the detection and the subsequent characterization of the orbital scissors mode [5–7].

The knowledge about spin and orbital motion in nuclei can be further enriched by the study of magnetic quadrupole ($M2$) transitions. Indeed, the spin component of the $M2$ operator induces relative displacements between spin-up and spin-down nucleons giving rise to spin-dipole excitations. Its orbital part correlates the relative displacement of the protons with their magnetic orbits generating the so called *twist* mode. Such a mode, predicted for spherical nuclei in a fluid-dynamic model [8,9], can be viewed as arising from a mutual rotation among different layers of the nuclear fluid around the z axis by an angle proportional to the z coordinate. Since no restoring force would be generated by such a rotation in an ideal fluid, the observation of such a mode would indicate that the nucleus behaves as an elastic medium.

Experimentally, electron scattering is specially suitable for a clean and complete study of $M2$ transitions. These experiments, however, do not distinguish between orbital and spin motion. One has, therefore, to rely also on theoretical analyses.

The few experimental data available until recently [10–14] showed that the $M2$ spin strength is fragmented and even more quenched than in the $M1$ case. Theoretical investigations were carried out in several approaches [15–32]. Some of them were devoted to the study of the *twist* mode [22–24,29]. It was found that for a correct description of the $M2$ spectra it is necessary to go beyond the random-phase approximation (RPA) by coupling one-particle–one-hole ($1p$-$1h$) to two-particle–two-hole ($2p$-$2h$) configurations. Such a coupling, while leaving the orbital strength distribution almost unchanged, induces a pronounced fragmentation of the spin strength [23]. A quite important and promising advance toward the understanding of the nature of the $M2$ transitions and the identification and characterization of the *twist* mode has been made recently by von Neumann-Cosel *et al.* [33]. In a high-resolution electron scattering experiment, they have determined the $M2$ strength distribution in ^{40}Ca and ^{90}Zr and analyzed the spectra by means of calculations carried out in second RPA that accounts for the coupling with the $2p$-$2h$ space. They found that the quenching of the $M2$ spin-dipole strength is comparable to the $M1$ case. Moreover, they showed that the orbital contribution is appreciable and crucial for the reproduction of the experimental data. This would therefore be a strong indirect evidence of the existence of the *twist* mode.

All experimental and theoretical studies were focused on heavy spherical nuclei. The $M2$ transitions in heavy deformed nuclei have attracted little attention. To our knowledge, this subject was touched only in [30] and confined to low-lying $M2$ spectra. On the other hand, there are good reasons to study $M2$ transitions in deformed nuclei. Since the possibility of detecting the twist mode relies on the separation of the orbital from the spin-dipole excitations, it is of interest to check if the, probably selective, fragmentation of the orbital and the spin $M2$ strengths induced by deformation favors such a splitting. In a strict sense, axial deformed nuclei should be ideal systems for the occurrence of the orbital *twist* mode. In fact, they provide naturally their symmetry axis as rotational axis for such a motion.

There is another aspect that links $M2$ transitions to deformation. Given their analogy to the electric dipole excitations, we might expect a splitting of the $M2$ strength induced by deformation similar to the one observed for the $E1$ giant resonance [34].

In this paper we carry out a study of the $M2$ transitions by adopting a strength-function technique developed for proton-neutron quasiparticle RPA in the signature formalism [35]. This technique avoids lengthy diagonalizations and therefore allows to cover the full-energy range of the $M2$ transitions.

We adopt a two-body potential composed of dipole and spin-dipole separable pieces. This choice enables us to carry a unified study of both $E1$ and $M2$ spectra and to point out possible analogies between the two modes. In the case of deformed nuclei it allows to study possible interferences between electric and magnetic channels. Due to the simple structure of the interaction, we are able to test the sensitivity of spin dipole and orbital $M2$ spectra to the strength of the interaction. This latter issue is quite relevant to the possible identification of the *twist* mode, which relies on the separation between the two different excitation modes. We do not include explicitly the $2p$-$2h$ configurations. We account for the spreading of the strength by smoothing the transition lines through the use of a Lorentzian weight in the strength function.

II. BRIEF OUTLINE OF THE PROCEDURE

We give a brief outline of the procedure developed in Ref. [35] to derive the strength function for the simple case of one electric and one magnetic multipole fields. In this case, the Hamiltonian adopted has the structure

$$H = H_{\rm sp} + V_{\rm pair} + V_E + V_M . \tag{2.1}$$

$H_{\rm sp}$ is a deformed axially symmetric one-body Hamiltonian, $V_{\rm pair}$ the monopole pairing interaction, V_E and V_M are the electric multipole and magnetic spin-multipole separable two-body potentials of the form

$$V_E = -\frac{\chi_E}{2}[M^{(n)\dagger}_{\lambda\mu}M^{(n)}_{\lambda\mu} + M^{(p)\dagger}_{\lambda\mu}M^{(p)}_{\lambda\mu}] - \frac{\chi^{(np)}_E}{2}[M^{(n)\dagger}_{\lambda\mu}M^{(p)}_{\lambda\mu} + M^{(p)\dagger}_{\lambda\mu}M^{(n)}_{\lambda\mu}],$$

$$V_M = -\frac{\kappa_M}{2}[S^{(n)\dagger}_{l\lambda'\mu}S^{(n)}_{l\lambda'\mu} + S^{(p)\dagger}_{l\lambda'\mu}S^{(p)}_{l\lambda'\mu}] - \frac{\kappa^{(np)}_M}{2}[S^{(n)\dagger}_{l\lambda'\mu}S^{(p)}_{l\lambda'\mu} + S^{(p)\dagger}_{l\lambda'\mu}S^{(n)}_{l\lambda'\mu}]. \tag{2.2}$$

The multipole and spin-multipole fields $M^{(\tau)}_{\lambda\mu}$ and $S^{(\tau)}_{l\lambda\mu}$ ($\tau = n,p$) have the form

$$M^{(\tau)}_{\lambda\mu} = r^\lambda Y_{\lambda\mu}(\hat{r}),$$

$$S^{(\tau)}_{l\lambda\mu} = r^l[\sigma \otimes Y_l(\hat{r})]_{\lambda\mu} . \tag{2.3}$$

The strength constants are related to the isoscalar and isovector corresponding strengths by

$$\chi_E = \chi_\lambda[0] + \chi_\lambda[1], \quad \chi^{(np)}_E = \chi_\lambda[0] - \chi_\lambda[1],$$

$$\kappa_M = \kappa_{l\lambda}[0] + \kappa_{l\lambda}[1], \quad \kappa^{(np)}_M = \kappa_{l\lambda}[0] - \kappa_{l\lambda}[1]. \tag{2.4}$$

Multipole and spin-multipole fields of good signature were constructed, so as to allow for the extension of the technique to fast rotating nuclei, and, accordingly, the Goodman basis [36] was adopted. Pairing was treated in BCS approximation. The RPA formalism was developed so as to attain the separation of the spurious state by setting their energies to zero. When a single field is considered as in the schematic case, the RPA equations are turned into dispersion equations by a straightforward procedure (see, for instance, [37]). Following an analogous procedure also for our more general Hamiltonian we get a homogeneous system of four equations in the unknowns R_i,

$$\left(F^{(n)}_{M,M} - \frac{1}{2\kappa_M}\right)R_1 + \xi_M F^{(n)}_{M,M}R_2 + F^{(n)}_{M,E}R_3 + \xi_E F^{(n)}_{M,E}R_4 = 0,$$

$$\xi_M F^{(p)}_{M,M}R_1 + \left(F^{(p)}_{M,M} - \frac{1}{2\kappa_M}\right)R_2 + \xi_E F^{(p)}_{M,E}R_3 + F^{(p)}_{M,E}R_4 = 0,$$

$$F^{(n)}_{M,E}R_1 + \xi_M F^{(n)}_{M,E}R_2 + \left(F^{(n)}_{E,E} - \frac{1}{2\chi_E}\right)R_3 + \xi_E F^{(n)}_{E,E}R_4 = 0,$$

$$\xi_M F^{(p)}_{M,E}R_1 + F^{(p)}_{M,E}R_2 + \xi_E F^{(p)}_{E,E}R_3 + \left(F^{(p)}_{E,E} - \frac{1}{2\chi_E}\right)R_4 = 0. \tag{2.5}$$

In the above equations we have put

$$\xi_M = \frac{\kappa^{(np)}_M}{\kappa_M}, \quad \xi_E = \frac{\chi^{(np)}_E}{\chi_E},$$

and

$$F^{(\tau)}_{X,X} = \sum_{i,k\in\tau} \frac{(\varepsilon_i + \varepsilon_k)\tilde{f}^X_{ik}\tilde{f}^X_{ik}}{(\varepsilon_i + \varepsilon_k)^2 - \omega^2}, \quad X = M,E, \tag{2.6}$$

$$F^{(\tau)}_{M,E} = \sum_{i,k\in\tau} \frac{\omega\tilde{f}^M_{ik}\tilde{f}^E_{ik}}{(\varepsilon_i + \varepsilon_k)^2 - \omega^2}, \tag{2.7}$$

where

$$\tilde{f}^E_{ik} = i^{-(\mu+1)}\langle i|M_{\lambda\mu}|k\rangle(u_i v_k + u_k v_i), \tag{2.8}$$

$$\tilde{f}^M_{ik} = i^{-(\mu+1)}\langle i|S_{l\lambda\mu}|k\rangle(u_i v_k - u_k v_i).$$

Nontrivial solutions of the equations system are obtained from the request that the determinant of the corresponding matrix vanishes. One may notice that the electric dipole or magnetic quadrupole channels are mutually coupled. Because of the proton-neutron formalism, the matrix so obtained is not symmetric. A simple trick, however, has enabled us to turn this matrix into a new one $\hat{D}$ of symmetric form, so as to enforce the strength function technique [35].

Dealing with axially symmetric nuclei at low rotational frequencies, we have assumed the strong-coupling limit to be valid and adopted the total wave function

$$|\nu K^\pi IM\rangle = \sqrt{\frac{2I+1}{16\pi^2(1+\delta_{K0})}}[\mathcal{D}^I_{MK}(\theta)|\Phi_{\nu K^\pi}\rangle + (-1)^I\mathcal{D}^I_{M-K}(\theta)R_1|\Phi_{\nu K^\pi}\rangle], \tag{2.9}$$

where

$$|\Phi_{\nu K^\pi}\rangle = \mathcal{Q}^{(r)\dagger}_{\nu K^\pi}|0\rangle = \sum_{kl} [\psi^{\nu}_{kl}\beta^\dagger_k\beta^\dagger_{\bar{l}} - \varphi^{\nu}_{kl}\beta_k\beta_{\bar{l}}]|0\rangle \tag{2.10}$$

is the one-phonon intrinsic state corresponding to the νth RPA root. For $K^\pi = 0^\pi$, the intrinsic state is an eigenfunction of the signature operator R_1 with eigenvalue $r=(-)^I$. The total wave function then becomes

$$|\nu K^\pi = 0^\pi I = M = 0\rangle = \mathcal{Q}^{(r)\dagger}_{\nu K^\pi = 0^\pi}|0\rangle. \tag{2.11}$$

For such a K, only angular momenta I fulfilling the condition $r=(-)^I$ are allowed. This implies that signature and parity coincide or are opposite according to whether the transition is electric or magnetic, respectively. In our case, the negative signature $K^\pi = 0^-$ states ($I=1,3,5,\ldots$) describe the $K^\pi = 0^-$ branch of the giant $E1$ resonance (proton-neutron oscillation along the axial symmetry axis). The positive signature $K^\pi = 0^-$ bands ($I=0,2,4,\ldots$) contribute to the $K^\pi = 0^-$ branch of the giant $M2$ resonance and describe spin-dipole oscillations along the symmetry axis or the orbital twist mode. In a strict sense, the geometrical picture underlying the *twist* mode applies only to the $K^\pi = 0^-$ mode. Our aim was to compute the strength function

$$\begin{aligned}\mathcal{S}(\omega; X\lambda, K^\pi) &\approx \mathcal{S}_\Delta(\omega; X\lambda, K^\pi) \\ &= \sum_\nu B_\nu(X\lambda, K^\pi)\,\rho_\Delta(\omega-\omega_\nu),\end{aligned} \tag{2.12}$$

where $\rho_\Delta(\omega-\omega_\nu)$ is a weight for the reduced probability

$$\begin{aligned}B_\nu(X\lambda, K^\pi) &= B(X\lambda; gr \to \nu K^\pi I) \\ &= \frac{2}{1+\delta_{K0}}\delta_{\lambda I}|\langle\Phi_{\nu\pi K^\pi}|\mathcal{M}(X\lambda, \mu=K)|0\rangle|^2\end{aligned} \tag{2.13}$$

of the transition from the ground (gr) to an excited state with quantum numbers $\{\nu K^\pi I\}$. In the long wavelength limit, the multipole operators, of electric ($X=E$) or magnetic ($X=M$) type, are

$$\mathcal{M}(E\lambda\mu) = \sum_{i=1}^{A} e^{(\lambda)}_{eff}(i) r_i^\lambda Y_{\lambda\mu}(\hat{r}_i), \tag{2.14}$$

$$\begin{aligned}\mathcal{M}(M\lambda\mu) = \frac{\mu_N}{2}\sqrt{\lambda(2\lambda+1)}\sum_{i=1}^{A} r_i^{\lambda-1}\Big(& g^{(\lambda)}_{s,eff}(i) \\ & \times [\sigma_i \otimes Y_{\lambda-1}(\hat{r}_i)]_{\lambda\mu} + g^{(\lambda)}_{l,eff}(i)\frac{4}{\lambda+1} \\ & \times [l_i \otimes Y_{\lambda-1}(\hat{r}_i)]_{\lambda\mu}\Big),\end{aligned} \tag{2.15}$$

where $e^{(\lambda)}_{eff}(i)$ is the nucleon effective charge of multipolarity λ, μ_N is the nuclear magneton, $g^{(\lambda)}_{s,eff}(i)$ and $g^{(\lambda)}_{l,eff}(i)$ are the effective spin and orbital gyromagnetic ratios, respectively.

The weighting factor $\rho_\Delta(\omega-\omega_\nu)$ fulfills the conditions

$$\int_{-\infty}^{+\infty} dx\,\rho_\Delta(x) = 1, \quad \lim_{\Delta\to 0}\rho_\Delta(x) = \delta(x). \tag{2.16}$$

It is usually taken of Gaussian or Lorentzian form. The two options yield similar results [38]. Consistently with previous works [38–40], we chose a function of the Lorentzian form

$$\rho_\Delta(x) = \frac{\Delta}{2\pi}\frac{1}{x^2 + \left(\frac{\Delta}{2}\right)^2} \tag{2.17}$$

that has only two simple poles. By virtue of this choice, the strength function came out to be the result of the integral of a function $f(z)$ around the poles $z=\omega_\nu$, being ω_ν the RPA roots. Since the function fulfills the condition $\lim_{|z|\to\infty} f(z) = 0$, we could substitute the integral around the RPA poles with the sum of integrals around all other poles taken with opposite sign. The final outcome (see Ref. [35] for details) was

$$\begin{aligned}\mathcal{S}(\omega; X\lambda, K^\pi) = & -\frac{2}{\pi}\mathrm{Im}\frac{\det(\hat{B}(z))}{\det(\hat{D}(z))}\Big|_{z=\omega+i\Delta/2} \\ & + \frac{\Delta}{2\pi}\sum_{ij}(p^X_{ij})^2\Bigg[\frac{1}{[(\varepsilon_i+\varepsilon_j)-\omega]^2 + \frac{\Delta^2}{4}} \\ & - \frac{1}{[(\varepsilon_i+\varepsilon_j)+\omega]^2 + \frac{\Delta^2}{4}}\Bigg].\end{aligned} \tag{2.18}$$

In the above formula, ε_i are the quasiparticle energies and p^X_{ij} are the single-particle matrix elements of the $E1$ or $M2$ operators, the term $\det(\hat{D}(z))$ denotes the determinant of the symmetrized RPA secular matrix $\hat{D}$, while $\det(\hat{B}(z))$ is the determinant of a matrix $\hat{B}(z)$ that can be obtained by simply adding to the RPA matrix $\hat{D}(z)$ a first row and column with terms involving the electric or magnetic transition operator. For the electric transitions we have ($B_{11}=0$)

$$\begin{aligned}B_{21} &= \mathcal{F}^{(n)}_{E,M} + \xi_M\mathcal{F}^{(p)}_{E,M}, \quad B_{31} = \xi_M\mathcal{F}^{(n)}_{E,M} + \mathcal{F}^{(p)}_{E,M}, \\ B_{41} &= \mathcal{F}^{(n)}_{E,E} + \xi_E\mathcal{F}^{(p)}_{E,E}, \quad B_{51} = \xi_E\mathcal{F}^{(n)}_{E,E} + \mathcal{F}^{(p)}_{E,E}.\end{aligned} \tag{2.19}$$

For the magnetic ones we obtain ($B_{11}=0$)

$$\begin{aligned}B_{21} &= \mathcal{F}^{(n)}_{M,M} + \xi_M\mathcal{F}^{(p)}_{M,M}, \quad B_{31} = \xi_M\mathcal{F}^{(n)}_{M,M} + \mathcal{F}^{(p)}_{M,M}, \\ B_{41} &= \mathcal{F}^{(n)}_{M,E} + \xi_E\mathcal{F}^{(p)}_{M,E}, \quad B_{51} = \xi_E\mathcal{F}^{(n)}_{M,E} + \mathcal{F}^{(p)}_{M,E}.\end{aligned} \tag{2.20}$$

The quantities $\mathcal{F}^{(\tau)}_{X,Y}$ are

$$\mathcal{F}^{(\tau)}_{X,X} = \sum_{i,k\in\tau}\frac{(\varepsilon_i+\varepsilon_k)p^X_{ik}f^X_{ik}}{(\varepsilon_i+\varepsilon_k)^2 - \omega^2}, \quad X = M,E, \tag{2.21}$$

$$\mathcal{F}^{(\tau)}_{M,E}=\sum_{i,k\in\tau}\frac{\omega p^{M}_{ik}f^{E}_{ik}}{(\varepsilon_i+\varepsilon_k)^2-\omega^2},$$

$$\mathcal{F}^{(\tau)}_{E,M}=\sum_{i,k\in\tau}\frac{\omega p^{E}_{ik}f^{M}_{ik}}{(\varepsilon_i+\varepsilon_k)^2-\omega^2}.$$

They can be derived from the corresponding expressions (2.6) and (2.7) by replacing one of the matrix elements f^{X}_{ik} given by Eqs. (2.8) with the corresponding matrix elements p^{X}_{ik} of the electric ($X=E$) and magnetic ($X=M$) multipole operators given by Eqs. (2.15).

The first term on the right-hand side of Eq. (2.18) results from integrating along a path that encloses the poles $z=\omega\pm i\Delta/2$ of the Lorentzian function. The second one is obtained from integrating along a path enclosing the poles $z=\pm(\varepsilon_i+\varepsilon_j)$ for all possible quasiparticle indexes i,j. The first piece accounts for the interaction while the second gets the contribution coming from the unperturbed single-particle spectrum. *No RPA roots appear in Eq. (2.18).* This is a crucial point. It implies, in fact, that the strength function $\mathcal{S}(\omega;X\lambda,K^{\pi})$ can be determined *without* solving the RPA eigenvalue equations. One has to know only the quasiparticle energies ε_i and the matrix elements of the multipole fields.

Once we have evaluated the strength function, it is immediate to compute the non-energy- and energy-weighted sum of the $E1$ or the $M2$ strengths by simply computing the integral

$$S_n(X\lambda,K^{\pi})=\int_0^{\infty}\omega'^{n}\mathcal{S}(\omega';X\lambda,K^{\pi})d\omega'$$

$$=\sum_{\nu}\omega_{\nu}^{n}B_{\nu}(X\lambda,K^{\pi})\quad(n=0,1).\qquad(2.22)$$

For the energy-weighted sum the values obtained from the above equation can be compared with the corresponding ones derived from the double commutator,

$$S_1(X\lambda,K^{\pi})=\frac{1}{2}\langle 0|[\mathcal{M}^{\dagger}(X\lambda,K),[H,\mathcal{M}(X\lambda,K)]]|0\rangle.\qquad(2.23)$$

One can also easily compute the photoabsorption cross section. For the $E1+M2$ transitions we have simply

$$\sigma_K(\omega)=\frac{32\pi^3\alpha}{9e^2}\left[\omega\mathcal{S}(\omega;E1,K)+\frac{3}{100(\hbar c)^2}\omega^3\mathcal{S}(\omega;M2,K)\right]$$

$$=0.4023\omega\mathcal{S}(\omega;E1,K)+0.3428\ 10^{-8}\omega^3\mathcal{S}(\omega;M2,K),$$

where $\sigma_K(\omega)$ is in fm^2, $\mathcal{S}(\omega;E1,K)$ in e^2 fm^2 MeV^{-1} and $\mathcal{S}(\omega;M2,K)$ in μ_N^2 fm^2 MeV^{-1}.

III. NUMERICAL CALCULATIONS AND RESULTS

A. Details of the calculation

We adopted a Nilsson one-body potential with standard parameters [41] and took into account all major shells up to $N_{\max}=7$. This space is adequate for our purposes. As we shall see, the $E1$ and $M2$ energy-weighted sum rules considered in the paper are satisfied. We included a proton-proton and neutron-neutron pairing interaction with the pairing constants fixed so as to reproduce the mass differences. We then added a two-body separable interaction of the form (2.2) with electric dipole and magnetic spin-dipole fields

$$\hat{M}^{(\tau)}_{1\mu}=rY_{1\mu}(\hat{r}),$$

$$\hat{S}^{(\tau)}_{1\lambda\mu}=r[\sigma\otimes Y_1(\hat{r})]_{\lambda\mu}.$$

We do not include a spin-octupole interaction. Such a term should be present in principle. Indeed, the structure of the electromagnetic multipole moments suggests a spin-multipole field of the form

$$\hat{S}^{(\tau)}_{\lambda\mu}=\vec{\sigma}\cdot\nabla(f_{\lambda}(r)Y_{\lambda\mu}),\qquad(3.1)$$

which, for $\lambda=2$, yields in general a spin-dipole and a spin-octupole term. Having adopted a Nilsson one-body potential, however, we took consistently a field with no radial nodes and put

$$f_{\lambda}(r)=r^{\lambda}.\qquad(3.2)$$

Under this zero-node assumption, the spin-octupole component vanishes. It is also to be noticed that the spin-octupole component disappears also from the $M2$ operator in the long wavelength limit considered here. As we shall argue in the concluding remarks (Sec. IV), the inclusion of a spin-octupole interaction would have been irrelevant for our purposes in any case.

The chosen interaction couples magnetic and electric channels for $K^{\pi}=0^-,r=-1$ and $K^{\pi}=1^-,r=\pm1$. The isoscalar constant $\chi_1[0]$ of the dipole-dipole interaction was fixed by the request of getting a vanishing value for the lowest RPA root so as to decouple the spurious translational oscillation mode from the physical intrinsic states. We have indeed checked that the strength of the center-of-mass coordinate is concentrated at zero energy. The isovector dipole constant $\chi_1[1]$ was chosen so as to reproduce as close as possible the energies of the $E1$ peaks. The above procedure yielded $\chi_1[0]=0.049$ MeV fm^{-2} and $\chi_1[1]=-0.085$ MeV fm^{-2} for the spherical ^{144}Sm. In the deformed ^{154}Sm we got K-dependent constants χ_{1K}, namely, $\chi_{10}[0]=0.039$ MeV fm^{-2} and $\chi_{10}[1]=-0.071$ MeV fm^{-2} for $K^{\pi}=0^-$, $\chi_{11}[0]=0.047$ MeV fm^{-2} and $\chi_{11}[1]=-0.10$ MeV fm^{-2} for $K^{\pi}=1^-$. The isovector constants can be compared with the values deduced from the formula derived in schematic models [42]

$$\chi_{10}[1]=\frac{\pi V_1}{A\langle r^2\rangle}(1-\tfrac{4}{3}\delta)\simeq 472A^{-5/3}(1-\tfrac{4}{3}\delta)\ \text{MeV fm}^{-2},$$

$$\chi_{11}[1]=\frac{\pi V_1}{A\langle r^2\rangle}(1+\tfrac{2}{3}\delta)\simeq 472A^{-5/3}(1+\tfrac{2}{3}\delta)\ \text{MeV fm}^{-2}, \tag{3.3}$$

having put $V_1=130$ MeV. In the spherical case ($\delta=0$) our values are slightly smaller than the ones deduced from these formulas. In the deformed case, our $K=0$ strength is close to the value deduced from the above formula, while the $K=1$ constant is somewhat weaker.

The available experimental data do not allow to fix the strength constants of the spin-dipole interaction. We have therefore adopted the formula

$$\kappa_\sigma=\kappa_{1\lambda}[0]=\kappa_{1\lambda}[1]=c_0\frac{4\pi}{\langle r^2\rangle}\frac{25}{A} \tag{3.4}$$

borrowed from Ref. [16] apart from the factor c_0 that we included in order to allow for variations in the strength constant so as to study the sensitivity of the $M2$ response to the spin-dipole interaction. As indicated in the above equation, we have assumed equal values for isoscalar and isovector strengths. This is a common practice. Some authors, however, have assumed a vanishing, or negligible, isoscalar constant [18]. The two options yield results that are similar and, therefore, equivalent for our purposes.

In computing the $E1$ transition strength we chose for the effective charges the values

$$e_{eff}=-\frac{1}{2}\left(\tau_3-\frac{N-Z}{A}\right)e$$

that accounts for the recoil effect [39]. For ^{154}Sm the above formula yields $e^{(p)}_{eff}=0.597e$ and $e^{(n)}_{eff}=-0.403e$. For the $M2$ transitions we took the gyromagnetic factors $g^{(\tau)}_{s,eff}=0.7g^{(\tau)}_{s,free}$ and $g^{(\tau)}_{l,eff}=g^{(\tau)}_{l,free}$.

Our calculations have shown that, even in deformed nuclei, the $E1$ strength function is completely unaffected by the spin-dipole interaction and is sensitive solely to the dipole-dipole interaction that pushed the unperturbed resonance upward in energy by about 7 MeV. The $M2$ transitions are insensitive to the dipole-dipole interaction and respond only to the spin-dipole interaction. We have therefore studied separately electric dipole and magnetic quadrupole responses.

B. $E1$ giant resonance

We computed the $E1$ photoabsorption cross section for the spherical ^{144}Sm and the deformed ^{154}Sm nuclei and compared with experiments [34]. In the spherical ^{144}Sm we got one broad peak that follows closely the experimental data for a Lorentzian width $\Delta=2$ MeV (top panel of Fig. 1). In the deformed ^{154}Sm, the resonance is split into two bumps as requested by the experiments (bottom panel of Fig. 1). For the $\Delta=2$ MeV, the two peaks are smooth and reach their maxima at the observed energies. On the other hand, the calculation underestimates the experimental low-lying peak and overestimates the high-lying one. Since the first is entirely due to the $K^\pi=0^-$ excitations and the second solely due to the $K^\pi=1^-$ transitions, we can partly improve the agreement with experiments by adopting a larger Lorentzian width for computing the $K^\pi=1^-$ strength function. By doing so, we implicitly assume that the coupling with the $2p$-$2h$ configurations induces a larger spreading of the $K^\pi=1^-$ strength. The resulting profile of the cross section is indeed closer to the experimental one (upper panel of Fig. 2). This reflects the fact that, because of the larger spreading of the $K^\pi=1^-$ strength, the overlap between the $K^\pi=1^-$ and $K^\pi=0^-$ bumps has been enhanced (bottom panel of Fig. 2). Even with these new widths, however, the computed cross section is smaller at low and larger at high energy, though to a less extent.

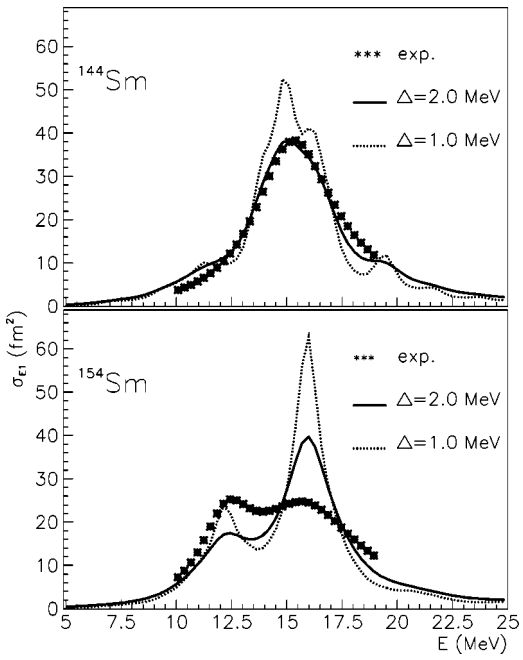

FIG. 1. Theoretical versus experimental $E1$ cross sections in ^{144}Sm (upper panel) and ^{154}Sm (bottom). The computations were made for two Lorentzian widths.

A key for a partial removal of the discrepancy may be found by observing that the fragmentation of the $E1$ strength in deformed nuclei is due not so much to the coupling with the $2p$-$2h$ configurations, but is the result of the dramatic increase of the density of the single-particle levels. How such a large density of states enhances the fragmentation of the strength can be inferred from the analysis of the energy-weighted sum rule (Table I). The computed quantities can be compared with the values obtained from the Thomas-Reich-Kuhn sum rule

$$S_1(E1,K^\pi=0^-)=\frac{1}{2}S_1(E1,K^\pi=1^-)=\frac{3}{8\pi}\frac{\hbar^2}{m}\frac{NZ}{A}e^2 \tag{3.5}$$

that accounts only for the one-body Hamiltonian. In the spherical ^{144}Sm the sum is slightly lower than the sum-rule value. In the deformed ^{154}Sm, the energy-weighted sum of the $E1$ strengths computed up to 30 MeV, is

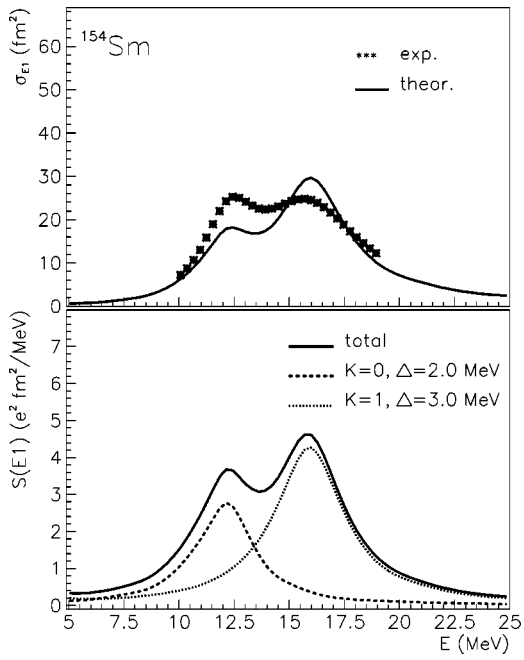

FIG. 2. Theoretical and experimental $E1$ cross sections in ^{154}Sm (upper panel) and the unfolding of the corresponding computed $E1$ strength function into the $K^\pi=0^-$ and $K^\pi=1^-$ contributions (bottom). Different widths were used for the two K^π transitions.

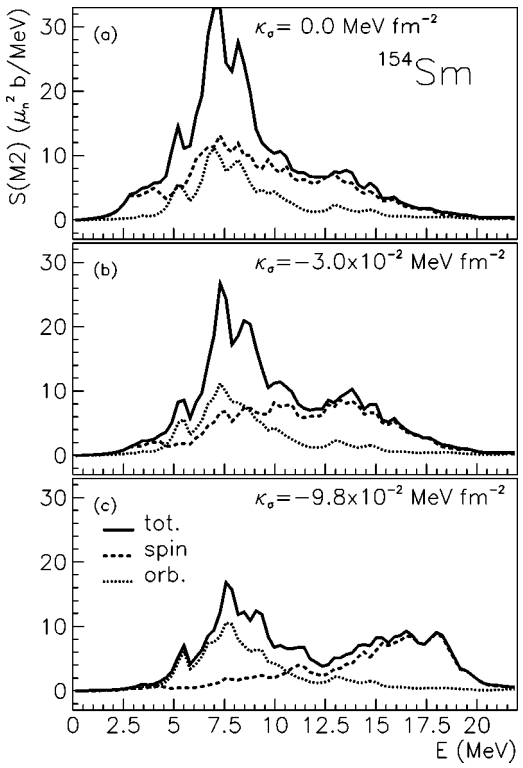

FIG. 3. The orbital, spin and total $M2$ strength functions in ^{154}Sm computed for increasing values of the spin-dipole interaction.

$S_1(E1)=518\ e^2\,\mathrm{fm}^2\,\mathrm{MeV}$ and increases to $S_1(E1)=539\ e^2\,\mathrm{fm}^2$ Mev if computed up 50 Mev. This latter number is close to the sum-rule value. Apparently, deformation induces a strong fragmentation of the strength. More in detail, the computed $K^\pi=0^-$ sum is appreciably smaller than the corresponding sum-rule value, while the $K^\pi=1^-$ sum is larger. It seems, therefore, that we need a modest redistribution of the strength among the single-particle levels that allows for the transfer of a small part of the strength from the $K^\pi=0^-$ to the $K^\pi=1^-$ transition lines.

We must also point out that our calculation does not account for contributions coming from exchange mixtures of the two-body interaction, so that the comparison with the total photoabsorption cross section is not completely appropriate specially at high energy.

C. $M2$ transitions

1. Interplay between orbital and spin-dipole transitions

The sensitivity of the $M2$ spectrum to the spin-dipole interaction is illustrated in Figs. 3 for ^{154}Sm. The unperturbed strength function exhibits one peak that results from the constructive interference between the orbital and the spin-dipole transition amplitudes [Fig. 3(a)]. The corresponding strengths are almost equally fragmented and spread over the same energy range around a common centroid. Only, the spin strength is larger and dominant at high energy. As we turn on the interaction, the orbital spectrum is practically unaffected. The spin-dipole strength, instead, gets more fragmented and quenched and is shifted at higher energy [Fig. 3(b)]. When the coupling constant of the interaction reaches the value normally adopted in literature [16] and obtained from Eq. (3.4) for $c_0=1$, the $M2$ strength function splits into two separate peaks, one at low energy around 7.5 MeV and another at high energy with a broad maximum extending from 15 to 18 MeV [Fig. 3(c)]. The first is almost entirely of orbital nature, the second is utterly due to spin-dipole excitations.

TABLE I. Energy-weighted sums of the $E1$ reduced strengths. The corresponding sum rule values obtained from Eq. (3.5) are in parentheses.

	^{144}Sm	^{154}Sm
$S_1(E1,K=0)(e^2\,\mathrm{fm}^2\,\mathrm{MeV})$	172 (175)	153 (183)
$S_1(E1,K=1)\ (e^2\,\mathrm{fm}^2\,\mathrm{MeV})$	344 (350)	386 (367)
$S_1^{(tot)}(E1)(e^2\,\mathrm{fm}^2\,\mathrm{MeV})$	516 (525)	539 (550)

The complete overlap between orbital and spin-dipole strength in the unperturbed case proves that the splitting has little to do with deformation. It is induced solely by the spin-dipole interaction. Indeed, also in the spherical ^{144}Sm (Figs. 4) we get overlapping orbital and spin-dipole spectra in the absence of interaction and an increasing splitting between the two as we increase the strength of the interaction. Deformation has the effect only of inducing more fragmentation. In fact the peaks are broad in the deformed ^{154}Sm and much sharper in the spherical ^{144}Sm. In both nuclei, the interaction does not affect the orbital strength distribution and has a severe quenching effect on the spin-dipole transitions.

The results obtained are compatible with the available experimental data. We computed the $M2$ strength function in

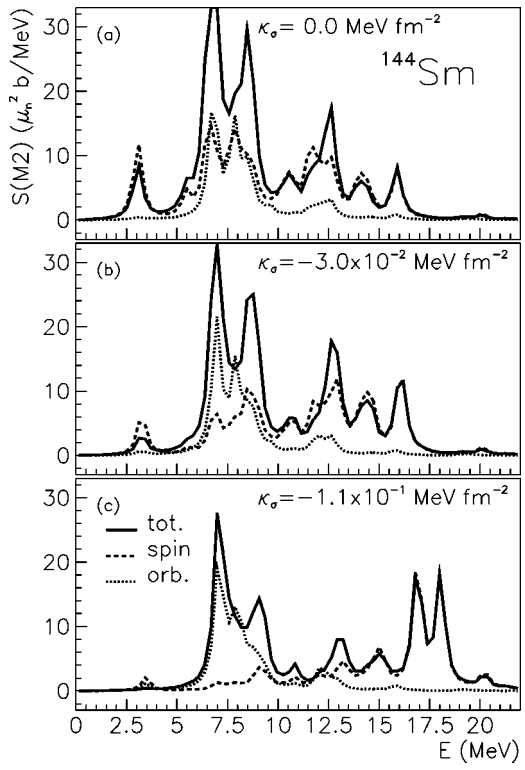

FIG. 4. The same as in Fig. 3 but for ^{144}Sm.

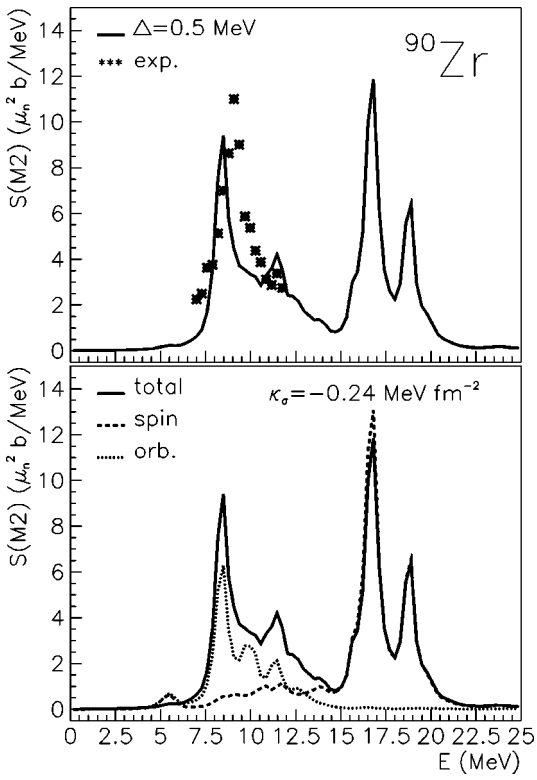

FIG. 5. Theoretical and experimental $M2$ strength function in ^{90}Zr (top) and its spin and orbital content (bottom).

^{90}Zr for two values of the spin-dipole strength. In both cases, we reproduced fairly well the electron scattering data [33] (top panel of Figs. 5 and 6). Maybe the larger coupling constant seems to do better, at least in the higher energy part of the experimental spectrum. In our opinion, however, the comparison does not allow a clear-cut discrimination between the two choices. On the other hand, using a larger or smaller constant is not a neutral choice. In the first case, the spin contribution to the strength is negligible (bottom panel of Fig. 5). The observed low-lying $M2$ transitions should therefore be viewed as a mere manifestation of the orbital *twist* mode. In the second case instead, the spin contribution, though smaller than the orbital one, is appreciable (bottom panel of Fig. 6) and *contaminates* the *twist* character of the $M2$ peak. This second spectrum would be more consistent with the findings of the analysis carried out in Ref. [33], where different one-body and two-body potentials were adopted.

Our calculation predicts strong spin-dipole transitions at higher energies packed around some high peaks. Experimental information on these excitations would probably enable us to fix the spin-dipole strength constant and therefore to make a more reliable assessment on the exact nature of the observed low-lying $M2$ peaks. The analysis of the available experimental data carried out here allows to state that, for any choice of the spin-dipole constant, the orbital motion gives a large contribution to the observed low-lying $M2$ strength distribution and plays a primary role in shaping the $M2$ spectrum and in determining the magnitude of the strength. We therefore fully support the findings of Ref. [33].

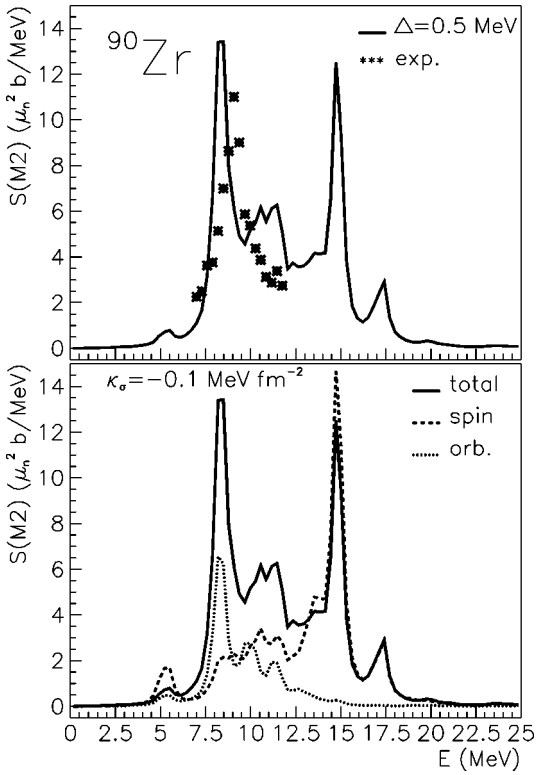

FIG. 6. The same as in Fig. 5 but for a smaller spin-dipole coupling constant.

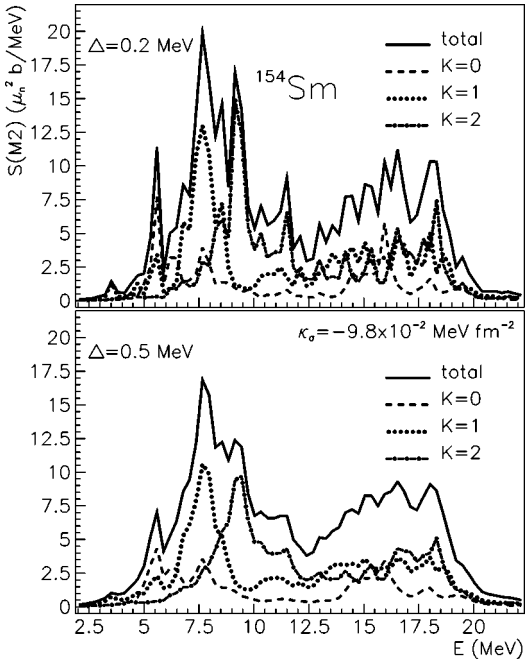

FIG. 7. The unfolding of the RPA $M2$ strength function in ^{154}Sm into its K^{π} components.

2. Splitting of the M2 strength in deformed nuclei

The effects of deformation become manifest if we carry out a fine-tuned analysis of the $M2$ spectrum in ^{154}Sm. Since the results are similar for a wide range of values of the spin-dipole constant, we present only those obtained by adopting the standard one. In the low-lying bump one may notice three distinct peaks falling around the energy centroids (Fig. 7). These are almost completely split for the Lorentzian width $\Delta=0.2$ MeV (top panel of Fig. 7). The nature of these peaks is easily understood once we unfold the bump into its K components. The $K^{\pi}=0^{-}$ strength is concentrated mostly in the lowest energy peak at $E_{0^-}\simeq 5.5$ MeV, the $K^{\pi}=1^{-}$ transitions generate the middle peak at $E_{1^-}\simeq 7.5$ and the $K^{\pi}=2^{-}$ ones the upper peak at $E_{2^-}\simeq 9.5$ (Fig. 7). This fine-tuned splitting of the $M2$ resonance reflects the close correspondence between electric dipole and magnetic quadrupole transitions. Indeed, in the unperturbed case we have schematically

$$B(M2,gr\rightarrow K^{\pi}=0^{-})\propto\langle 0|\left(\sum_i z(i)l_z(i)\right)^2|0\rangle$$

$$=\sum_{a\Lambda}\langle a\Lambda|z^2|a\Lambda\rangle\Lambda^2, \tag{3.6}$$

where a stand for all required quantum numbers. Since l_z does not yield any energy change, for our heuristic argument we can replace Λ^2 with a mean value $\overline{\Lambda^2}$. We then get

$$B(M2,gr\rightarrow K^{\pi}=0^{-})\propto\langle z^2\rangle\propto\frac{\omega^2}{\omega_z^2}\langle r^2\rangle. \tag{3.7}$$

Accounting for the fact that the energy change induced by l_{+1} is negligible compared to $\hbar\omega$, we can make the same simplifying assumption also for the other K transitions obtaining

$$B(M2,gr\rightarrow K^{\pi}=2^{-})\propto\langle r_{\perp}^2\rangle\propto\frac{\omega^2}{\omega_{\perp}^2}\langle r^2\rangle,$$

$$B(M2,gr\rightarrow K^{\pi}=1^{-})\propto\langle z^2\rangle+\langle r_{\perp}^2\rangle\propto\left(\frac{\omega^2}{\omega_{\perp}^2}+\frac{\omega^2}{\omega_z^2}\right)\langle r^2\rangle\simeq\langle r^2\rangle. \tag{3.8}$$

According to the equations written above, the $K=0$ and the $K=2$ $M2$ components, in perfect analogy to the $K=0$ and the $K=1$ $E1$ operators, excite p-h states around $\hbar\omega_z\simeq\hbar\omega(1-2/3\delta)$ and $\hbar\omega_{\perp}\simeq\hbar\omega(1+1/3\delta)$, respectively. The $K^{\pi}=0^{-}$ and the $K^{\pi}=2^{-}$ $M2$ excitations are therefore the analog of the $K=0$ and the $K=1$ $E1$ modes. The $M2$ operator, however, through the $K=1$ component, excites other levels around the energy $\hbar\omega$. These levels fall between the $K^{\pi}=0^{-}$ and the $K^{\pi}=2^{-}$ peaks and therefore tend to fill the gap between them. This heuristic procedure yield for the centroids of the different K transitions the values $E_{0^-}\simeq 6.3$ MeV, $E_{1^-}\simeq 7.6$ MeV, and $E_{2^-}\simeq 8.3$ MeV. They are close to the energies obtained in the full calculations. We may notice an appreciable discrepancy only for the $K^{\pi}=2^{-}$ case. On the whole, the agreement is quite satisfactory, given the rough nature of the schematic estimate.

Mainly because of the $K^{\pi}=1^{-}$ intruders, the splitting of the low-lying, mainly orbital, $M2$ resonance is not as pronounced as in the $E1$ giant resonance. Nonetheless, the splitting should be observed in high-resolution (e,e') scattering experiments. In such a case, in a strict sense, we would be able to identify the twist mode as the low-lying $K^{\pi}=0^{-}$ transition lines enveloped into the lowest peak and, moreover, to distinguish this from the other K modes. All these excitations, however, have alike properties. For instance all of them are sensitive only to the one-body potential. We, therefore, prefer to consider all three K^{π} peaks on the same footing. In the most pessimistic hypothesis of insufficient experimental resolution, the splitting should get manifest indirectly as a broadening of the resonance with respect to the spherical case. This would be the analog of the broadening of the $E2$ giant resonance in deformed nuclei [43].

No K splitting is obtained in the region of the spin excitations. We observe, in fact, a large overlap between the energy domains of the different K transitions. Apparently, the K regularities we would have expected on the ground of the schematic model are wiped out by the large fragmentation of the strength induced by the high density of the single-particle states. Also the use of the same coupling constant for all K channels, at variance with the case of the $E1$ giant resonance, contributes to destroy these regularities.

3. Running sums and sum rule analysis

The global properties of the $M2$ transitions can be studied efficiently by computing the running sum of the correspond-

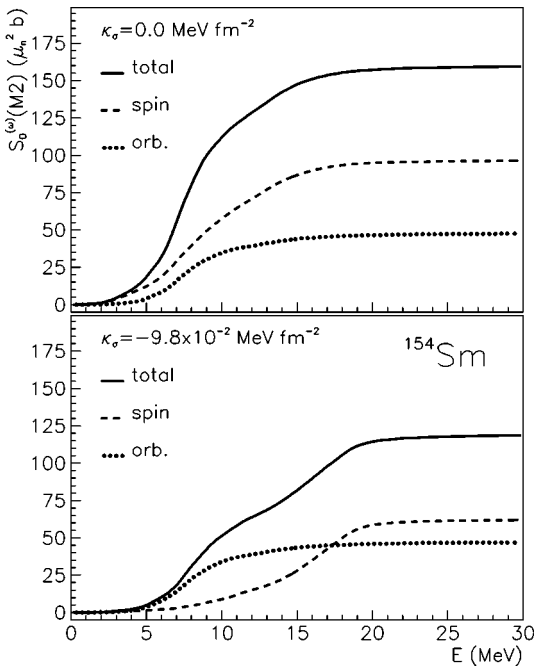

FIG. 8. The orbital, spin and total nonenergy-weighted running sum of the $M2$ reduced strength in ^{154}Sm in the absence (top) and in the presence (bottom) of the spin-dipole interaction.

ing reduced strengths. This can be extracted from the strength function through the use of the formula

$$S_n^{(\omega)}(M2,K)=\int_0^\omega \omega'^n \mathcal{S}(\omega';M2,K)d\omega'=\sum_\nu^\omega \omega_\nu^n B_\nu(M2,K). \tag{3.9}$$

The plot in Fig. 8 for ^{154}Sm shows that, in the unperturbed case, orbital and spin strengths grow almost together up to the saturation point of the orbital strength. From this point on, only the spin strength keeps growing smoothly until it reaches the plateau around 16–17 MeV. The spin-dipole running sum is larger than the orbital one at any energy. In the presence of the interaction, the orbital running sum remains unchanged. The spin sum, instead, increases slowly up to a small value in the domain of the orbital transitions and then raises rapidly to a saturation value that is only slightly larger than the corresponding orbital sum. The quenching effect of the interaction on the spin-dipole transitions is thereby clearly proven. The same trend is observed in the spherical ^{144}Sm. Only the rising of both strengths is sharper. Qualitatively similar results are obtained for the energy-weighted running sum. Only, the saturation value of the spin sum is much higher because of the energy weight that privileges the spin excitations falling at higher energies.

The asymptotic values of the running sums coincide with the total nonenergy- and energy-weighted sums. These are shown in Table II for the spherical ^{90}Zr and ^{144}Sm and the deformed ^{154}Sm. The summed strengths grow as we move from ^{90}Zr to the heavier ^{144}Sm and ^{154}Sm. This is especially true for the orbital transitions. The orbital strength is about 30% of the total in ^{90}Zr and about 40% in Sm isotopes. The increasing importance of the orbital motion with increasing A was expected since in heavier nuclei higher angular momenta are involved. It confirms earlier suggestions [23] that the heavier the nucleus the easier it should be to identify the twist mode. No appreciable differences are noticeable in going from the spherical ^{144}Sm to the deformed ^{154}Sm.

TABLE II. Nonenergy- and energy-weighted sums of the $M2$ reduced strengths. In parentheses the orbital energy-weighted sum rule values obtained from Eq. (3.11).

	^{90}Zr	^{144}Sm	^{154}Sm
$S_0^{(l)}(M2)$ ($\mu_N^2 b$)	14.7	40.8	46.9
$S_0^{(\sigma)}(M2)$ ($\mu_N^2 b$)	30.3	57.5	61.9
$S_0^{(tot)}(M2)$ ($\mu_N^2 b$)	47.7	103.6	118.5
$S_1^{(l)}(M2)$ ($\mu_N^2 b$ MeV)	142 (139)	349 (350)	425 (428)
$S_1^{(\sigma)}(M2)$ ($\mu_N^2 b$ MeV)	487	868	913
$S_1^{(tot)}(M2)$($\mu_N^2 b$ MeV)	651	1251	1413

The energy-weighted sums can be compared with the corresponding sum-rule values obtained by computing the double commutator of Eq. (2.23) for the $M2$ operator. We will do this for the orbital motion that is more interesting for our purposes. The calculation yields for the different K transitions

$$S_1(M2,K=0)=\frac{5}{2\pi}\frac{\hbar^2}{m}\langle 0|\sum_{k=1}^{Z} l_z^2(k)|0\rangle,$$

$$S_1(M2,K=1)=\frac{5}{6\pi}\frac{\hbar^2}{m}\langle 0|\sum_{k=1}^{Z} [3l_z^2(k)+l^2(k)]|0\rangle,$$

$$S_1(M2,K=2)=\frac{5}{3\pi}\frac{\hbar^2}{m}\langle 0|\sum_{k=1}^{Z} [2l^2(k)-3l_z^2(k)]|0\rangle. \tag{3.10}$$

Contrary to the $E1$ energy weighted sum rule that is independent of deformation [Eq. (3.5)], the $M2$ sum is K dependent. It is easy to check that the three sums converge to a common expression in the spherical limit. It is easy to check as well that the total sum rule has the same form for both spherical and deformed nuclei

$$S_1(M2)=\frac{25}{6\pi}\frac{\hbar^2}{m}\langle 0|\sum_{k=1}^{Z} l^2(k)|0\rangle. \tag{3.11}$$

A rather detailed comparison between the energy-weighted sums and the corresponding sum-rule values is presented in Table III for ^{154}Sm. One may observe from this and Table II that the computed orbital $M2$ strengths fully satisfy the sum rule in both spherical and deformed nuclei. Concerning the deformed ^{154}Sm (Table III), the orbital sum rule is satisfied for each K. Consistent with Eqs. (3.10), the sum changes appreciably with K. By contrary the spin-dipole sums are the same for all K. This was also expected since, for instance, the contribution to the spin-dipole sum rule coming from the kinetic energy is

TABLE III. Nonenergy- and energy-weighted sums of the $M2$ reduced strengths ^{154}Sm for different K quantum numbers. The orbital energy-weighted sum rule values obtained from Eqs. (3.10) are in parentheses.

	$K^\pi=0^-$	$K^\pi=1^-$	$K^\pi=2^-$	Sum over K's
$S_0^{(l)}(M2)$ $(\mu_N^2 b)$	7.7	19.1	20.1	46.9
$S_0^{(\sigma)}(M2)$ $(\mu_N^2 b)$	12.8	24.9	24.2	61.9
$S_0^{(tot)}(M2)$ $(\mu_N^2 b)$	22.7	47.8	48.1	118.5
$S_1^{(l)}(M2)$ $(\mu_N^2 b$ MeV)	55.0 (56.4)	163.4 (166.0)	206.3 (206.1)	424.7(428.4)
$S_1^{(\sigma)}(M2)$ $(\mu_N^2 b$ MeV)	187.3	364.3	361.1	912.7
$S_1^{(tot)}(M2)(\mu_N^2 b$ MeV)	253.0	557.8	602.0	1413.0

$$S_1^{(\sigma)}(M2,K^\pi=0^-)=\frac{5}{8\pi}\frac{\hbar^2}{m}(g_p^2 Z+g_n^2 N) \qquad (3.12)$$

for $K^\pi=0^-$ and is the same for the other K quantum numbers. This expression is quite similar to the corresponding $E1$ energy-weighted sum [Eq. (3.5)].

IV. CONCLUSIONS

Our calculation shows that the interference between dipole and spin-dipole channels induced by deformation is negligible. $E1$ and $M2$ strength functions can therefore be computed separately using dipole-dipole and spin-dipole interactions, respectively. As regards the $M2$ transitions, the spin-dipole response is very sensitive to the interaction. This, by contrary, does not affect the orbital excitations, which, beyond any underlying geometrical picture, represent a remarkable example of collisionless mode in nuclei. Because of the different sensitivity of the two modes to the interaction, the shape of the resulting $M2$ spectrum depends strongly on its intensity. Independently of deformation, the orbital and spin-dipole strengths overlap or get split according that the coupling constant of the spin-dipole interaction is weaker than or comparable to the value normally adopted in literature. In the latter case the orbital $M2$ mode would be almost completely separated and would be easily identified. For any value of the spin-dipole strength constant, however, the orbital contribution to the total $M2$ strength at low energy is comparable if not stronger than the spin-dipole one. We therefore support the conclusion of the analysis made in Ref. [33].

We may make the more compelling statement that, in virtue of the constructive interference between orbital and spin $M2$ amplitudes, the theoretical orbital strength should provide a lower bound for the magnitude of the measured $M2$ strength. The theoretical uncertainties on such a bound should come only from the single-particle basis adopted. In fact, it is very difficult to think of any quenching mechanism for the orbital transitions, given their insensitivity to the interaction. The measured low-lying $M2$ strength should therefore be larger than the theoretical orbital $M2$ strength. The difference between the two should come only from the spin transitions in the same energy domain and, therefore, should give useful information on the spin-dipole coupling constant. Such a constant would be completely determined if the experiments could cover the high-energy range so as to allow for a thorough comparative analysis of the $M2$ spectrum.

Deformation does not play a major role in the interplay between orbital and spin motion. On the other hand, it induces a K splitting of the orbital $M2$ strength analogous to the one observed in the $E1$ giant resonance. The separation between the peaks is smaller than in the $E1$ resonance mainly because of the *intrusion* of the $K^\pi=1^-$ component, which does not have an electric counterpart, between the $K^\pi=0^-$ and $K^\pi=2^-$ peaks, corresponding respectively, to the $E1$ $K^\pi=0^-$ and the $K^\pi=1^-$excitations. Such a splitting should be nonetheless observable in high-resolution (e,e') scattering experiments.

The main conclusions drawn on the ground of the present results should remain valid even if we extend the calculation scheme so as to allow for the coupling with the $2p$-$2h$ configurations. The explicit inclusion of these configurations, while leaving the orbital $M2$ strength distribution basically unchanged [23], should have the effect of quenching and fragmenting the spin strength. We have actually accounted for such a fragmentation in an effective way through the width entering into the Lorentzian weight of the strength function.

We expect these conclusions to hold also if we replace the Nilsson with a Woods-Saxon potential and include a spin-octupole interaction. The spin-octupole interaction is expected to leave the $M2$ orbital spectrum unchanged and to push the $M2$ spin strength further up in energy, thereby enforcing our conclusions. The Woods-Saxon potential will certainly modify the strength distribution. The induced changes, however, should be of minor importance in the low-energy part of the spectrum and, therefore, should not invalidate our main results.

ACKNOWLEDGMENTS

The work was partly supported by the Prin 99 of the Italian MURST (N.L. and P.A.), the Czech Republic Grant No. 202/99/1718 (J.K. and A.M.), and the RFBR Grant No. 00-0217194 (V.O.N.)

[1] For a short review see A. Richter, Prog. Part. Nucl. Phys. **34**, 261 (1995).
[2] T. Wakasa *et al.*, Phys. Rev. C **55**, 2909 (1997).
[3] T. Wakasa *et al.*, Phys. Lett. B **426**, 257 (1998).
[4] B. Reitz *et al.*, Phys. Rev. Lett. **82**, 291 (1999).
[5] N. Lo Iudice and F. Palumbo, Phys. Rev. Lett. **41**, 1532 (1978).
[6] D. Bohle *et al.*, Phys. Lett. **137B**, 27 (1984).
[7] For a review and references see for instance N. Lo Iudice, Phys. Part. Nucl. Phys. **28**, 556 (1997).
[8] G. Holzwarth and G. Eckart, Z. Phys. A **283**, 219 (1977).
[9] G. Holzwarth and G. Eckart, Nucl. Phys. **A325**, 1 (1979).
[10] R. Frey *et al.*, Phys. Lett. **74B**, 45 (1978).
[11] D. Meuer *et al.*, Nucl. Phys. **A349**, 309 (1980).
[12] D. Meuer *et al.*, Phys. Lett. **106B**, 289 (1981).
[13] D. Müller *et al.*, Phys. Lett. **113B**, 362 (1982).
[14] C. Lüttge *et al.*, Nucl. Phys. **A606**, 183 (1996).
[15] P. Ring and J. Speth, Phys. Lett. **44B**, 477 (1973).
[16] B. Castel and I. Hamamoto, Phys. Lett. **65B**, 27 (1976).
[17] W. Knüpfer *et al.*, Phys. Lett. **77B**, 367 (1978).
[18] V. Yu. Ponomarev, V.G. Soloviev, Ch. Stoyanov, and A.I. Vdovin, Nucl. Phys. **A323**, 446 (1979).
[19] V. Yu. Ponomarev, Phys. Lett. **97B**, 4 (1980).
[20] J. Speth, V. Klemt, J. Wambach, and G.E. Brown, Nucl. Phys. **A343**, 382 (1980).
[21] K. Goeke and J. Speth, Annu. Rev. Nucl. Part. Sci. **32**, 65 (1982).
[22] B. Schwesinger, K. Pingel, and G. Holzwarth, Nucl. Phys. **A341**, 1 (1980).
[23] B. Schwesinger, Phys. Rev. C **29**, 1475 (1984).
[24] V. Yu. Ponomarev, J. Phys. G **10**, L177 (1984).
[25] N. Auerbach and A. Klein, Phys. Rev. C **30**, 1032 (1984).
[26] D. Cha *et al.*, Nucl. Phys. **A430**, 321 (1984).
[27] D. Cha and J. Speth, Phys. Rev. C **29**, 636 (1984).
[28] T.S. Dumitrescu and T. Suzuki, Nucl. Phys. **A423**, 277 (1984).
[29] S.I. Bastrukov and V.V. Gudkov, Z. Phys. A **341**, 395 (1992).
[30] V.G. Soloviev and N.Yu. Shirikova, Yad. Fiz. **55**, 2359 (1992) [Sov. J. Nucl. Phys. **55**, 1310 (1992)].
[31] F. Osterfeld, Rev. Mod. Phys. **64**, 491 (1992).
[32] N. Tsoneva *et al.*, Phys. At. Nucl. **61**, 734 (1998).
[33] P. von Neumann-Cosel *et al.*, Phys. Rev. Lett. **82**, 1105 (2000).
[34] S.S. Dietrich and B. L. Berman, At. Data Nucl. Data Tables **38**, 200 (1988).
[35] J. Kvasil, N. Lo Iudice, N.O. Nesterenko, and M. Kopal, Phys. Rev. C **58**, 209 (1998).
[36] A. Goodman, Nucl. Phys. **A230**, 466 (1974).
[37] D.J. Rowe, *Nuclear Collective Motion* (Methuew, London, 1970).
[38] L.A. Malov, preprint R4-81-228, 1981.
[39] A. Bohr and B.R. Mottelson, *Nuclear Structure II* (Benjamin, New York, 1969).
[40] L.A. Malov, V.O. Nesterenko, and V.G. Soloviev, Teor. Mat. Fiz. **32**, 134 (1977) [Theor. Math. Phys. **32**, 646 (1977)].
[41] A.K. Jain *et al.*, Rev. Mod. Phys. **62**, 393 (1990).
[42] T. Suzuki and D.J. Rowe, Nucl. Phys. **A289**, 461 (1977).
[43] T. Kishimoto *et al.*, Phys. Rev. Lett. **35**, 552 (1975).